



HAL
open science

Hippocampal effective synchronization values are not pre-seizure indicator without considering the state of the onset channels.

Farzaneh Shayegh, Saeed Sadri, Rassoul Amirfattahi, Karim Ansari-Asl, Jean-Jacques Bellanger, Lotfi Senhadji

► To cite this version:

Farzaneh Shayegh, Saeed Sadri, Rassoul Amirfattahi, Karim Ansari-Asl, Jean-Jacques Bellanger, et al.. Hippocampal effective synchronization values are not pre-seizure indicator without considering the state of the onset channels.: Inability of synchronization values as pre-seizure. Network: Computation in Neural Systems, 2014, 25 (4), pp.139-167. 10.3109/0954898X.2014.940409 . inserm-01062400

HAL Id: inserm-01062400

<https://inserm.hal.science/inserm-01062400>

Submitted on 4 Oct 2014

HAL is a multi-disciplinary open access archive for the deposit and dissemination of scientific research documents, whether they are published or not. The documents may come from teaching and research institutions in France or abroad, or from public or private research centers.

L'archive ouverte pluridisciplinaire **HAL**, est destinée au dépôt et à la diffusion de documents scientifiques de niveau recherche, publiés ou non, émanant des établissements d'enseignement et de recherche français ou étrangers, des laboratoires publics ou privés.

Hippocampal Effective Synchronization Values are not Pre-seizure Indicator without Considering the State of the Onset Channels

F Shayegh^{1,4}, S Sadri¹, R Amirfattahi¹, K Ansari-Asl², J. J. Bellanger³ and L. Senhadji³

¹Digital Signal Processing Lab, Department of Electrical and Computer Engineering, Isfahan University of Technology, 84156-83111, Isfahan, Iran

²Shahid Chamran University, Ahvaz, Iran

³Laboratoire Traitement du Signal et de L'Image, INSERM, Université de Rennes 1, Campus de Beaulieu, 35042 Rennes Cedex, France

⁴Department of Electrical Engineering, Payam Noor University, Isfahan, Iran

E-mail: farzaneh.shayegh@gmail.com, sadri@cc.iut.ac.ir, fattahi@cc.iut.ac.ir

Corresponding Author:

Farzaneh Shayegh

Digital Signal Processing Lab, Department of Electrical and Computer Engineering, Isfahan University of Technology, 84156-83111, Isfahan, Iran

Payam-Noor University, Isfahan, Iran

Tel: +989133173220

farzaneh.shayegh@gmail.com

Running Title: Inability of synchronization values as pre-seizure

30 Pages

6 Tables

10 Figures

12 Equations

The total number of words: (i) the whole manuscript: 7719; (ii) the Abstract: 265; and (iii) the Introduction: 1654.

Key words coupling, effective synchronization, seizure prediction, model-based, parameter identification

Abstract In this paper, a model-based approach is presented to quantify the effective synchrony between hippocampal areas from depth-EEG signals. This approach is based on the parameter identification procedure of a realistic Multi-Source/Multi-Channel (MSMC) hippocampal model that simulates the function of different areas of hippocampus. In the model it is supposed that the observed signals recorded using intracranial electrodes are generated by some hidden neuronal sources, according to some parameters. An algorithm is proposed to extract the intrinsic (solely relative to one hippocampal area) and extrinsic (coupling coefficients between two areas) model parameters, simultaneously, by a Maximum Likelihood (ML) method. Coupling coefficients are considered as the measure of effective synchronization. This work can be considered as an application of Dynamic Causal Modeling (DCM) that enables us to understand effective synchronization changes during transition from inter-ictal to pre-ictal state.

The algorithm is first validated by using some synthetic datasets. Then by extracting the coupling coefficients of real depth-EEG signals by the proposed approach, it is observed that the coupling values show no significant difference between ictal, pre-ictal and inter-ictal states, *i.e.*, either the increase or decrease of coupling coefficients has been observed in all states. However, taking the value of intrinsic parameters into account, pre-seizure state can be distinguished from inter-ictal state. It is claimed that seizures start to appear when there are seizure-related physiological parameters on the onset channel, and its coupling coefficient toward other channels increases simultaneously.

As a result of considering both intrinsic and extrinsic parameters as the feature vector, inter-ictal, pre-ictal and ictal activities are discriminated from each other with an accuracy of 91.33% accuracy.

Key words coupling, effective synchronization, seizure prediction, model-based connectivity, parameter identification

1. Introduction

Recently seizure prediction and detection based on EEG signals have attracted considerable attention. Some different bivariate and multivariate features have been shown to be powerful in discriminating seizure, pre-seizure and normal states. Synchronization between the signals of

different channels is one of the most predictive features applied in seizure prediction procedure. In fact, since seizure genesis has been attributed to abnormal synchronous firing of a large population of neurons, synchronization seems to be a suitable means for characterizing the seizure and pre-seizure states. In 2003, Mormann (Mormann et al., 2000; Mormann et al., 2003) showed a decrease in phase synchronization between EEG channels minutes before seizure. Then, Winterhalder (Winterhalder et al., 2006) claimed that although the pre-seizure dynamical change of synchronization values in EEG signals can be used for seizure prediction, the pathogenic mechanisms may be different for every channel, and both decrement and increment of synchronization could precede epileptic seizures, depending on the structures underlying each channel (Le Van Quyen et al., 2005). Afterward, the evidences for suitability of synchronization measures have been found only in small subgroups of all possible channel combinations and even in some special sub-bands (Chavez et al., 2003). But, yet no significant pre-ictal changes in the EEG signals' synchronization value have been reported (Jouy et al., 2005). Studies about the pattern of EEG synchronizations before and during seizure is still under investigation (Mirowski et al., 2009). Although synchronization values have been found to be different in pre-ictal and inter-ictal states, it has yet to be proven that it is sensitive and accurate enough for clinical use (Schelter et al., 2006). The synchronization measure must be studied more carefully, because, there may be no significant relation between inter-relation of brain areas and seizure appearance. The fact is that there is still an ongoing debate about the hyper-synchrony (Franaszczuk and Bergey, 1999) or hypo-synchrony (Frei et al., 2010; Netoff et al., 2002) nature of seizure genesis process.

In addition to the debate about the real hypo- or hyper-synchronous nature of the epileptic signals, there is also major disagreement about the measures used to quantify the amount of coupling between brain areas (Frei et al., 2010). Indeed, it is claimed that the aforementioned contradictory reports might be the result of using different methods of the synchronization quantification. Differences could also be attributed to different time and spatial scales being

studied. Conventional methods could measure statistical (functional) synchronization of brain areas, based only on the signals recorded from those areas. In (Ansari-Asl et al., 2006; Wendling et al., 2009), various developed methods in this context have been evaluated using different types of signals. It is shown that the performance of these methods depends essentially on the signal characteristics. Linear or nonlinear relation between signals and also the bandwidth of signals (narrow or broad) significantly influence the efficiency of these algorithms (Sakkalis et al., 2009), and none of the synchronization quantification conventional methods outperforms the others. In fact, these methods consider the signals from different statistical aspects such that each algorithm works well only for some types of signals (Ansari-Asl et al., 2006). One of the most common pitfalls of conventional synchronization measurement methods is to find no relation between signals despite the presence of their effective synchronization in a narrow band of frequency (Ansari-Asl et al., 2005). Another pitfall is to consider signals that are generated by uncoupled systems as synchronous signals, because of their similar activity at some specific frequencies. These drawbacks occur because usually, conventional measures are calculated just from the observed signals without considering their underlying sources (Pikovsky et al., 2001).

Recently, some attempts have been made to measure the effective synchronization between EEG signals based on utilizing a model of the underlying sources (Penny et al., 2009; David et al., 2006; Kiebel et al., 2006; Friston et al., 2012). Penny (Penny et al., 2009) supposed the signals as phase-coupled data and used a dynamic casual modeling (DCM) framework for their analysis: Dynamic phase changes of signals are attributed to the coupling variation between oscillators that generate signals. The best interrelation model of oscillators and the best parameters of the coupling have been obtained using the Bayesian approach. David et al., (2006) and Kiebel et al., (2006) used DCM for analyzing the evoked responses of brain to make inference about connectivity changes in the networks underlying EEG/MEG signals: Considering the brain as a network, and each area of the brain as a component of this network,

by using such approaches intrinsic and extrinsic connection parameters, propagation delays between areas, synaptic parameters that control the kinetics within an area, input parameters of the model, and spatial parameters of the sensors recording ERP signals have been estimated.

As well as the deterministic DCMs, appropriate for ensemble average signals that are (in mean field limit) deterministic, such as ERP signals, some stochastic DCMs are developed (Li et al., 2011; Friston et al., 2012). These stochastic DCMs can be used in order to quantify the effective synchronization of brain areas from random EEG signals in such a way that the functional synchronization (*e.g.*, cross-spectral characteristics) of signals is preserved. In stochastic DCMs, endogenous or random fluctuations in unobserved (hidden) neuronal and physiological sources have been allowed (Li et al., 2011). In other words, in these models, in order to analyze the brain areas' effective synchronization based on the observed signals, some hidden neuronal sources have been mapped to the observed EEG signals. This input/output mapping is usually done through some states, *i.e.* a state-space model. The hidden sources must be estimated (explicitly or implicitly) using a model inversion technique. Various attempts to perform the inversion more accurately (from observed signals to intrinsic and extrinsic parameters of model, and also the model states) have been undertaken. Generally the model inversion procedure has been done using Maximum Likelihood and/or Bayesian inference.

As well, in this paper, we aim to estimate the effective synchronization values between brain areas, using the DCM concept based on a stochastic generative model (Stephan et al., 2010) of depth-EEG signals (Wendling et al., 2000). In this model, each area of the hippocampus is separately modeled as a Single-Source Single-Channel (SSSC) system (Wendling et al., 2000), in which the neural sub-populations interact with each other through inhibitory or excitatory relations; and source signal is modeled by a white Gaussian noise. The SSSC model output is the sum of subpopulations' post synaptic potentials that resembles real depth-EEG signals neglecting the measurement noise. According to the dynamic causal relations of brain areas, this model is then extended to an Multi-Source Multi-Channel (MSMC) model in such a way

that the inter-relation between brain areas is comprised by taking the input of every area's SSSC model equal to the delayed and scaled versions of the potential of all other areas, in our case the SSSC model outputs (David and Friston, 2003). Hence, the MSMC has two kinds of parameters: the intrinsic and extrinsic ones. The former are the parameters of the SSSC model, and the latter are their coupling coefficients. This model can appropriately imitate the behavior of multi-channel epileptic depth-EEG signals. Thus, it is possible to estimate these parameters underlying an observed multi-channel depth-EEG signal through an identification procedure, *i.e.*, a model-inversion method.

One useful property of the MSMC model is the one-to-one mapping between the hidden neuronal source underlying each channel of observed depth-EEG signal and the signal itself, for each value of its intrinsic parameters. This property enables us to perform the main part of the ML-based model inversion procedure with deterministic approach. This property resolves the requirement of approximating the model states at every value of the intrinsic parameters, and thus reduces the model inversion errors. In other words, in this work, by selecting the MSMC model, we removed the usual necessity to mean-field approximation (Li et al., 2011); *i.e.*, assuming neuronal states and model parameters to be independent. Thus, with our technique, the hidden neuronal sources can be obtained deterministically. Nevertheless, since it is assumed that the hidden neuronal sources consist of a random fluctuation term to make the model stochastic, the ML method is required to find the most probable fluctuation term.

Shortly, in the ML-based estimation procedure proposed in this paper, both the optimal intrinsic parameters of the areas and the effective synchronization values between areas are obtained according to the multi-channel EEG signals: the “coupling matrix” containing the coupling coefficients between all possible pairs of recorded signals, which are directional values, is a measure of brain effective synchronization. This measure is more realistic than the conventional functional synchronization measures, because the signal generation mechanism is considered in it.

Ultimately, according to the advantages of the “coupling matrix”, we expect it could eliminate the ambiguities about the role of synchronization as a seizure precursor. To our knowledge, the present work for the first time uses stochastic DCM concept to infer changes of effective synchronization during seizure genesis.

The structure of the paper is as follows: At first, both SSSC and MSMC models and their output characteristics are described. Then, the ML parameter estimation algorithm for this model is illustrated and applied to synthetic depth-EEG signals to show the efficiency of the algorithm. Afterward, in order to obtain the coupling values between the possible pairs of the hippocampal areas underlying recorded depth-EEG signals of epileptic patients the proposed algorithm is applied to the signals available in Freiburg dataset. In the absence of the ground truth for the coupling values of the real signals, the small difference of the cross spectrum of the real signals and those of the corresponding estimated signals validates the efficiency of the algorithm. Then, according to this “coupling matrix” it is shown that effective synchronization of depth-EEG signals do not experience a significant difference during inter-ictal, pre-ictal and ictal states. So, the intrinsic values of the onset areas are considered, and it is shown that increment of the coupling coefficient of the onset areas towards other areas is an indicator of the future seizure, just when simultaneously, the onset areas have some special (seizure related) values of intrinsic parameters.

2. Methods: Model of Hippocampus

2.1. Local (SSSC) Model

An area of the hippocampus containing sub-populations of pyramidal neurons and interneurons has been modeled in different manners. All subpopulation models use two transforms, a nonlinear static function, $S(\cdot)$, followed by a linear dynamic one, whose impulse response is $h_a(t)$ (Wendling et al., 2002); these two transforms respectively convert the average pre-synaptic potential of that subpopulation, $v(t)$, to the average firing rate, $f(t) = S(v(t))$, (at the

synapse), and the average firing rate to post-synaptic potential, $o(t) = f(t) * h_a(t)$, (at the soma), as shown in Figure 1. These sub-populations of hippocampus interact with each other through inhibitory or excitatory relations. The pyramidal neurons are always modeled to have only excitatory effect, *i.e.*, they only have additive post-synaptic potentials; but the hippocampal interneurons, in different models, are modeled by different types of sub-populations. In reality, fast and slow inhibitory and also excitatory interneurons exist simultaneously. Considering all these three sub-populations of interneurons in the hippocampus ensures normal and epileptic activities, even the fast discharge activity at the model output (Da Silva et al., 1974).

Hence, a neuronal population with four sub-populations (pyramidal cells, excitatory, fast and slow inhibitory interneurons) driven by a white Gaussian noise, which simulates the effect of hidden neuronal sources, can reproduce depth-EEG signals. In fact, the effects of other brain areas (hidden neuronal states) are simulated by a white Gaussian noise. In more realistic models, other areas of brain like thalamus are also involved. But, the scope of this paper is limited to a pure hippocampal model. This model is illustrated in Figure 2. As depicted in this figure, for each sub-population the basis structure shown in Figure 1 is present in the model. Impulse response of the pyramidal cells' dynamic function is displayed by $h_a(t)$, and those of interneurons are displayed by $h_r(t)$, $h_b(t)$ and $h_g(t)$, respectively for excitatory, slow inhibitory and fast inhibitory interneurons.

This local model of the hippocampus can reproduce a single channel depth-EEG signal (Da Silva et al., 1974) as the sum of subpopulations' post synaptic potentials. In fact, in this paper the measurement noise is not considered since the SNR of recorded depth-EEG signals is sufficiently high, *i.e.*, the high SNR of depth-EEG signals allows us to accept the model outputs as recorded depth-EEG signals directly without any modification, even adding some measurement noise.

This model can be illustrated by the state space equations. The equation set (1) shows how the depth-

EEG signals are built from the input $u(t)$. The Ordinary Differential Equations (ODE) given in (1) represent a stochastic model due to its random input. Actually, it is just the model input that makes the model to be a stochastic one: because with zero hidden neuronal sources and with zero initial states, behavior of the model would be purely deterministic. Denoting the white Gaussian noise with $p(t)$, the abovementioned facts about the model input can be written in the form of: $u(t) = p(t)$. y_0 to y_9 are the states of the model, among which y_1 , y_2 and y_3 respectively stand for the excitatory, fast inhibitory and slow inhibitory post-synaptic potentials (EPSP, fast IPSP, slow IPSP) of the involved subpopulations (Figure 2). The nonlinear static function is a sigmoid one, *i.e.*, $S(v) = 2e_0 / [1 + e^{r(v_0 - v)}]$. However, the Euler numerical method is accurate enough to solve these ODEs (David and Friston, 2003).

$$\begin{aligned}
\dot{y}_0(t) &= y_5(t) \\
\dot{y}_5(t) &= A\tau S[y_1(t) - y_2(t) - y_3(t)] - 2\tau y_5(t) - \tau^2 y_0(t) \\
\dot{y}_1(t) &= y_6(t) \\
\dot{y}_6(t) &= Aa\{u(t) + C_2 S[C_1 y_0(t)]\} - 2ay_6(t) - a^2 y_1(t) \\
\dot{y}_2(t) &= y_7(t) \\
\dot{y}_7(t) &= BbC_4 S[C_3 y_0(t)] - 2by_7(t) - b^2 y_2(t) \\
\dot{y}_3(t) &= y_8(t) \\
\dot{y}_8 &= GgC_7 S[C_3 y_0(t) - C_6 y_4(t)] - 2gy_3(t) - g^2 y_3(t) \\
\dot{y}_4(t) &= y_9(t) \\
\dot{y}_9 &= BbS[C_3 y_0(t)] - 2by_4(t) - b^2 y_4(t) \\
y_{out}(t) &= y_1(t) - y_2(t) - y_3(t)
\end{aligned} \tag{1}$$

The adjustable SSSC model parameters that are excitatory gain, A , fast and slow inhibitory gains, B and G , and pyramidal excitatory time constant, τ , are gathered in a parameter vector $\theta = [A, B, G, \tau]$, hereafter called ‘‘intrinsic parameters’’. These parameters have been shown to be the most effective in modifying the activity type of the model output (Wendling et al., 2002; Shayegh et al., 2013). By changing the intrinsic parameters, θ , six types of activities can be

seen in the SSSC model output: normal background, sporadic spikes, sustained discharge of spikes, low voltage rapid activity, slow quasi-sinusoidal activity, and slow rhythmic activity. All of these activity types can be observed in the real normal or pathological signals (Wendling et al., 2002). The other parameters of linear system (C_1 to C_7, a, b, g) and nonlinear function parameters (e_0, v_0 and r) take their standard values according to (Wendling et al., 2002). These constant standard values are presented in Table 1.

It is noteworthy that although the dynamics of the model output signals are very similar to the real ones, this local model is not able to simulate the true dc value, and also the true range of depth-EEG signals. However, by normalizing the model output signals, the normalized depth-EEG signals can be reproduced by the model.

2.1.1. Characteristics of the SSSC model

According to (1), the SSSC model represents a nonlinear dynamic system. Analysis of its behavior requires bifurcation analysis. In the bifurcation analysis, appearance of different activities at the model output (as a function of parameter values) is attributed to the variation of the kind of system's equilibrium point, which may be a stable or non-stable fixed point or a limit cycle. Although this kind of analysis is beyond the scope of this paper, but it is noteworthy that for a few specific values of the parameter θ there would be more than one attractor in the phase space of the SSSC model, such that beginning from different initial points, the trajectory of the system's phase space may

converge to different attractors. In other words, for a particular value of θ , different activities may be seen at the model output. Excluding these rare situations, by considering zero-state response of the model (*i.e.*, when initial values of the states are set to zero) for each value of θ , the relation between input and output sequences seems to be one to one.

Proposition- Suppose that we set zero initial value for the state signals of equation set (1), *i.e.*, $y_i(0) = 0, i = 0, 1, \dots, 9$. Equation set (1) defines a one to one relation, at each value of θ , between N -point input and output signals. In other words, the defined $N \rightarrow N$ relation is an injective function.

Proof- In order to prove the one-to-one relation, we must show that:

$$i) \quad \text{If } \mathbf{u}_1^{1:N} = \mathbf{u}_2^{1:N} \Rightarrow \mathbf{y}_{out_1}^{1:N} = \mathbf{y}_{out_2}^{1:N}.$$

$$ii) \quad \text{If } \mathbf{u}_1^{1:N} \neq \mathbf{u}_2^{1:N} \Rightarrow \mathbf{y}_{out_1}^{1:N} \neq \mathbf{y}_{out_2}^{1:N}$$

where N points of the signal are considered as an N -dimensional vector. This is emphasized by the bold notation, *e.g.*, $\mathbf{u}_1^{1:N}$ stands for the model input involving N points of a white Gaussian noise; similarly $\mathbf{y}_{out}^{1:N}$ stands for the model output.

First, since filters of the model are linear at each parameter vector, and also $S(\cdot)$ is an injective function and \mathbf{y}_{out} is a linear combination of state signals, there is only one zero state response for each model input, and (1) is evident. Also, due to the abovementioned reasons, the model (1) is reversible. The equation set (2) shows the equations of the inverse model:

$$\begin{aligned} \ddot{y}_0(t) + 2\tau\dot{y}_0(t) + \tau^2 y_0(t) &= A\tau S[y_{out}(t)] \\ \ddot{y}_2(t) + 2b\dot{y}_2(t) + b^2 y_2(t) &= BbC_4 S[C_3] \\ \ddot{y}_4(t) + 2b\dot{y}_4(t) + b^2 y_4(t) &= BbS[C_3 y_0(t)] \\ \ddot{y}_3(t) + 2g\dot{y}_3(t) + g^2 y_3(t) &= GgC_7 S[C_3] \\ y_1(t) &= y_{out}(t) + y_2(t) + y_3(t) \\ u(A, B, G, \tau; y_{out}(t)) &= \frac{2\tau\dot{y}_1(t) + \tau^2 y_1(t)}{A\tau} \end{aligned} \quad (2)$$

According to (2), given two identical output signals $\mathbf{y}_{out_1}^{1:N} = \mathbf{y}_{out_2}^{1:N}$, the zero state responses of the model's inverse system would be the same at each parameter value $\theta = [A, B, G, \tau]$, *i.e.*,

$\mathbf{u}_1^{1:N}(\theta; \mathbf{y}_{out_1}^{1:N}) = \mathbf{u}_2^{1:N}(\theta; \mathbf{y}_{out_2}^{1:N})$; thus the second condition (ii) is satisfied; hence the equation (1) is a one-to-one relation. \square

It is noteworthy that in practice the equation sets (1) and (2) must be solved numerically. So it is important to choose a numerical method that does not destroy the one-to-one relation. The Euler method preserves this one-to-one relation, albeit after the convergence of the model outputs.

2.2. Global (MSMC) Model

As well as the single-channel depth-EEG signals, multi-channel signals can also be modeled. In order to generalize the SSSC model to a MSMC one, at first, each area of the hippocampus is separately modeled as the SSSC model (David and Friston, 2003). Then, the contribution of different areas of the hippocampus on the neuronal source of one area is modeled by adding delayed and scaled versions of the post synaptic potentials of other neural masses (*i.e.*, other SSSC model outputs) to the neuronal source of that area (Shayegh et al., 2014; Shayegh et al., 2013). Indeed, the input of each SSSC model is no longer a pure white noise, because a combination of other channels' depth-EEG signals is added to it (David and Friston, 2003). Consequently, as shown in equation (3), the neuronal source of each area consists of a deterministic term (the effect of the other areas from which depth-EEG signal is recorded) and a stochastic term (random fluctuations):

$$u_j(t) = p_j(t) + \sum_{\substack{i=1 \\ i \neq j}}^M c_{ji} O_i(t), \quad t=1, \dots, N \quad (3)$$

where u_j and O_j are denoted for the input and the normalized output signal of the j th SSSC model (*i.e.* j th area), respectively. The fluctuation term $p_j(t)$ at the input of j th area

represents the hidden influence of far areas of the brain whose activities are not recorded. Indeed, the contributions of these hidden sources are modeled by the white noise.

In this paper, the delays of propagation between neuronal populations are neglected (this assumption is acceptable for nearby areas). The scales are represented by coupling coefficients c_{ji} between pairs of depth-EEG signals. The parameter c_{ji} is the weight by which i th area influences the input of the j th area and is called the extrinsic parameter of the model. A schematic representation of the MSMC model is shown in Figure 3.

The parameters of an M -channel MSMC model (including both intrinsic and extrinsic parameters) can be formed as a $M \times (4 + (M - 1))$ dimensional matrix:

$$\Theta_M = \begin{bmatrix} \theta_1 & | & C_1 \\ \vdots & | & \vdots \\ \theta_M & | & C_M \end{bmatrix}, \theta_j = \begin{bmatrix} A_j \\ B_j \\ G_j \\ \tau_j \end{bmatrix}^T, C_j = \begin{bmatrix} c_{j1} \\ \vdots \\ c_{ji} \\ \vdots \\ c_{jM} \end{bmatrix}^T \quad \text{where } j \neq i \quad (4)$$

where θ_j is the intrinsic parameter vector of j th SSSC model.

While the SSSC model was able to simulate the effect of changing the seizure onset channel's intrinsic parameters on the seizure appearance (seizure initiation), via this MSMC model the propagation of seizure can be described. In fact, we suppose that seizures initiate in a few onset areas because of their intrinsic parameters' variation and propagate to other (*i.e.*, normal) areas because of the coupling between the areas. In other words, seizures do not propagate without coupling between areas, in such a way that there may be no clinical manifestations of seizures. However, it is yet not clear whether the coupling values change significantly before the seizure onset or not.

3. Methods: ML-estimation of MSMC Model Parameters

As implied in section 1, the Maximum Likelihood method can be used to estimate (identify) both intrinsic and extrinsic parameters underlying the multi-channel depth-EEG signals. For each channel of depth-EEG signal, the conditional distribution of the fluctuations term (random part) of that channel's corresponding source (*i.e.*, its hidden neuronal states) must be maximized. Since these fluctuation terms are modeled by white Gaussian noise, for j th area, the conditional distribution can be written as:

$$f_{p_j^{1:N}}(p_j^{1:N} | \theta_j, c_{ji}) = \frac{1}{(\sqrt{2\pi}\sigma_j)^N} \prod_{k=1}^N e^{-\frac{(p_j^k - \mu_j)^2}{\sigma_j^2}}, i = 1, \dots, M, j \neq i \quad (5)$$

where p_j^k denotes for k th sample of the fluctuation term of the j th area's input, which is modeled by a white Gaussian noise with the mean μ_j and variance σ_j . For the sake of generality, the mean and variance of different areas are assumed to be not similar.

On the other hand, according to the one-to-one property of the function of each SSSC model (the proposition of section 2.1.1), the source underlying the recorded signal of j th channel can be obtained at any intrinsic parameter value θ_j . This is done by solving the inverse ODEs; but before it, for each value of θ_j , the normalized observed depth-EEG signal ($\mathcal{O}_j^{1:N}$) must be modified in such a way that the $y_{out,j}^{1:N}$ take the dc value and range equal to those of the SSSC model output at θ_j . The input obtained in this manner for any intrinsic parameter value, θ_j , is called $\mathbf{u}_j^{1:N}(y_{out,j}^{1:N}; \theta_j)$. Since this source signal is modeled as (3), the fluctuations term of j th source can be written as follows:

$$\hat{\mathbf{p}}_j^{1:N}(y_{out,j}^{1:N}; \theta_j, c_{ji}) = \mathbf{u}_j^{1:N}(y_{out,j}^{1:N}; \theta_j) - \sum_{\substack{i=1 \\ i \neq j}}^M c_{ji} \mathcal{O}_i^{1:N}, \quad i = 1, \dots, M, j \neq i \quad (6)$$

By replacing (6) in (5), to identify all the unknown intrinsic and extrinsic parameters (θ_M) of j th channel, the optimization problem (7) must be solved:

$$\max_{\theta_j, C_j} \frac{1}{(\sqrt{2\pi}\sigma_j)^N} \prod_{k=1}^N \exp \left[-\frac{(\mathbf{u}_j^{1:N}(\mathbf{y}_{out,j}^{1:N}; \theta_j) - \sum_{\substack{i=1 \\ i \neq j}}^M c_{ji} \mathbf{O}_i^{1:N} - \mu_j)^2}{\sigma_j^2} \right], \quad i=1, \dots, M, j \neq i \quad (7)$$

By taking the logarithm of the cost function (7), the optimization equation would be reduced to:

$$\min_{\theta_j, C_j} J_j(\theta_j, C_j) \stackrel{\Delta}{=} \sum_{k=1}^N \left[\mathbf{u}^k(\mathbf{y}_{out,j}^{1:N}; \theta_j) - \sum_{i=1, j \neq i}^M c_{ji} \times \mathbf{O}_i^k - \mu_j \right]^2 \quad (8)$$

It is noteworthy that by using the normalized depth-EEG signals, just the dynamics of the signal influences the cost function (8). Evidently, normalization destroys some useful information of signal that can be helpful in the identification procedure. However, if the SSSC model could reproduce synthetic depth-EEG signals with such dc and amplitude value consistent to the real signals, more information of the real EEG signals would be available to estimate the model parameters.

3.1. Solution of the optimization problem

Computing the derivative of the cost function (8) with respect to $c_{ji}, i=1, \dots, M, i \neq j$, and then equating it to zero, leads to the following equation:

$$\frac{1}{2} \sum_{k=1}^N \left[u^k (\mathbf{y}_{out,j}^{1:N}; \theta_j) - \sum_{i=1, j \neq i}^M c_{ji} \times O_i^k - \mu_j \right] \times O_i^k = 0 \quad (9)$$

$$i = 1, 2, \dots, M, i \neq j$$

Thus, for a given intrinsic parameter vector θ_j , the relevant optimum values of coupling coefficients, $C_j^*(\theta_j)$, are obtained by solving the following set of linear equations:

$$\begin{bmatrix} \sum_{k=1}^N O_1^k \times O_1^k & \dots & \sum_{k=1}^N O_1^k \times O_M^k \\ \vdots & \ddots & \vdots \\ \sum_{k=1}^N O_M^k \times O_1^k & \dots & \sum_{k=1}^N O_M^k \times O_M^k \end{bmatrix} \times \begin{bmatrix} c_{j1}^*(\theta_j) \\ \vdots \\ c_{jM}^*(\theta_j) \end{bmatrix} = \begin{bmatrix} \sum_{k=1}^N O_1^k \times u^k (\mathbf{y}_{out,j}^{1:N}; \theta_j) \\ \vdots \\ \sum_{k=1}^N O_M^k \times u^k (\mathbf{y}_{out,j}^{1:N}; \theta_j) \end{bmatrix} \quad (10)$$

The value of cost function (8) at these optimum coupling coefficients, *i.e.*, $J_j(\theta_j, C_j^*(\theta_j))$ is a function of intrinsic parameters that we call $J_j^*(\theta_j)$. But, minimizing $J_j^*(\theta_j)$ is not possible through setting the derivatives to zero because it is not an explicit function of θ_j . Instead, a search algorithm, preferably a full search one, can be used to find the optimum intrinsic parameter θ_j^* . Correspondingly, the $C_j^*(\theta_j^*)$ will be selected as final value of the coupling coefficient vector.

In summary, in order to simultaneously obtain the intrinsic parameters of each hippocampal area and the directional coupling coefficients between every pair of the depth-EEG signals (extrinsic parameters), it is sufficient to do the following steps for every channel, $j = 1, \dots, M$:

- a. Normalize the signals to obtain $\mathbf{o}_j^{1:N}$ with zero mean and unit variance.
- b. For every θ_j :

i) after rescaling and shifting the $\mathcal{O}_j^{1:N}$ by the predefined values for θ_j , obtain $\mathbf{u}_j^{1:N}(\mathbf{y}_{out,j}^{1:N};\theta_j)$

ii) compute $C_j^*(\theta_j)$ through the following equation:

$$\begin{bmatrix} c_{j1}^*(\theta_j) \\ \vdots \\ c_{jM}^*(\theta_j) \end{bmatrix} = \text{inv} \left(\begin{bmatrix} \sum_{k=1}^N \mathcal{O}_1^k \times \mathcal{O}_1^k & \dots & \sum_{k=1}^N \mathcal{O}_1^k \times \mathcal{O}_M^k \\ \vdots & \ddots & \vdots \\ \sum_{k=1}^N \mathcal{O}_M^k \times \mathcal{O}_1^k & \dots & \sum_{k=1}^N \mathcal{O}_M^k \times \mathcal{O}_M^k \end{bmatrix} \right) \times \begin{bmatrix} \sum_{k=1}^N \mathcal{O}_1^k \times u^k(\mathbf{y}_{out,j}^{1:N};\theta_j) \\ \vdots \\ \sum_{k=1}^N \mathcal{O}_M^k \times u^k(\mathbf{y}_{out,j}^{1:N};\theta_j) \end{bmatrix} \quad (11)$$

iii) define $J_j^*(\theta_j) \stackrel{\Delta}{=} J_j(\theta_j, C_j^*(\theta_j))$.

c. find $\theta_j^* = \arg \min_{\theta_j} J_j^*(\theta_j)$ and let $C_j^* = C_j^*(\theta_j^*)$

Eventually, the coupling coefficients that constitute the off-diagonal elements of the $M \times M$ coupling matrix are taken as the depth-EEG signals' effective synchronization measure.

4. Validation of the Parameter Identification Algorithm

The main question of this paper is whether the couplings coefficients between brain areas change significantly before and/or during seizure genesis and propagation, or whether they remain unchanged. Thus, at first, to ensure the efficiency of the coupling measurement algorithm, the abovementioned procedure for estimation of coupling coefficients is applied to some synthetic signals.

The synthetic signals (of both seizure and normal type) have been generated by running the MSMC model. We supposed that for an epileptic patient, in the normal situations the intrinsic parameters of all areas of the hippocampus have values very close to the standard ones such that the SSSC model generates background EEG activity. As well, it is supposed that shortly before seizure occurrence, intrinsic parameters of some onset areas start to change gradually from their standard values to such values that can maintain sustained discharge of spikes, low

voltage rapid activity, slow rhythmic activity or quasi-sinusoidal activity on these areas, and the seizure then propagates to other areas of the hippocampus.

As an illustrative example, a 5-channel signal is considered here (Shayegh et al., 2014). Areas one and four are assumed to be the onset areas. An example of both seizure-like and normal signals is shown in Figure 4. Synthetic signals shown in Figure 4(a) are of normal type. In the seizure relevant signals, shown in Figure 4(b), the first and fourth channels are the focal area of seizure. The other three channels just get the seizure activity from the focal areas (because of coupling), while their intrinsic parameters do not alter significantly. In other words, seizures spread though brain because of the coupling between its areas.

In the present MSMC model, it is assumed that the parameters have constant values during an observed segment of signal, *i.e.*, the probable variations of parameters are not considered. So this model is only suitable for generating short segments of depth-EEG signals, for which the constant assumption of the parameters is physiologically justifiable.

The intrinsic parameter vectors underlying the five EEG channels shown in Figure 4(a) and 4(b) are displayed in Table 2, respectively, in super-rows 1 and 2. Extrinsic parameters of these signals, *i.e.*, coupling coefficients between channels, are displayed in Table 3. In Table 3 each coupling coefficient c_{ji} corresponds to the weight by which i th area influences the j th area (j and i are indexes of row and column, respectively). The coupling coefficients are selected to be asymmetric.

Each signal shown in Figure 4 is the result of running MSMC model just one time. In order to be able to do statistical analysis 199 other times, further synthetic signals are simulated with the values of first and second super-rows of Table 2 and Table 3. These datasets, each containing 200 signals, are called Dataset I and II.

By using the proposed algorithm described in section 3.1, for each synthetic signal of Datasets I and II the intrinsic and extrinsic parameters have been identified simultaneously. As a result, the mean and variance of the identified intrinsic and extrinsic parameters (for 200 runs) are

summarized in Tables 2 and 3, respectively. The identified parameters are very close to the original ones. For some values of θ the minimum of the cost function $J_j^*(\theta_j)$ is clearly distinct, such that in all 200 cases the identified parameters are exactly the same as the true ones, and there is zero variance. For other cases, the small bias and variance of the estimated values, which is evident from Tables 2 and 3, validates the efficiency of the identification algorithm. In other words, the identification algorithm appears to be able to effectively estimate the real value of both intrinsic parameters and coupling coefficients. To investigate the repeatability of the appropriate efficiency of the algorithm for different the intrinsic and extrinsic values, the abovementioned procedure has been repeated for three other sets (Datasets III to V). Each of these datasets contains the signals brought forth by 200 different runs of the MSMC model signal with different set of intrinsic and extrinsic parameters. It must be emphasized that no special limitations are considered in selecting these parameters, *i.e.*, signals were allowed to have any type of activities. The details of these parameters are not given in detail, but a summary of the identification algorithm's performance in estimating the parameters of all five datasets is displayed in Figure 5. In this figure, the bias and variance ranges of the estimations made for different intrinsic and extrinsic parameter values are rendered respectively in Figure 5(a) and (b). To be more specific, intrinsic parameters of all channels are shown altogether. Also, coupling values of every channel toward other channels are displayed together. The small values of the bias and variance for different amounts of parameters, as shown in Figure 5, imply that all of the parameters are accurately identified. Now, it is safe to mention that the proposed algorithm can successfully identify both intrinsic and extrinsic parameters, regardless their values. However, since the step (c) of the algorithm is an optimization algorithm, which is done using a full-search method on 4-D intrinsic parameter (θ_j) space, it takes too much to run the algorithm, *i.e.* practically the algorithm cannot be an online algorithm. The algorithm is now ready to be applied to real signals to estimate their coupling coefficients.

5. Implementation the Identification Algorithm to Real depth-EEG Signals

5.1. Real Signals

In this work, depth-EEG signals of FSPEEG database¹ (Shelter et al., 2006), recorded from eleven patients suffering from temporal lobe epilepsy are considered for investigation. Information about the recording procedure of FSPEEG data is given in <http://epilepsy.uni-freiburg.de>. In this database, the inter-ictal and ictal activities are available as separate records. The ictal activity records contain signals from a few minutes before seizure onset to approximately five minutes after seizure termination.

The onset and termination times of each seizure are also indicated in the database. The number of recorded depth-EEG signal channels varies for different patients; therefore, in order to obtain comparable results, we only use the signals from six patients (among the eleven patients) for whom at least three depth-EEG channels are available. Configuration of the selected three channels is such that they include two in-focus channels and one out-of-focus channel.

It is noteworthy that the drawbacks of using such few channels is compensated by inserting the fluctuation term in the hidden neuronal sources of MSMC model as the contribution of the hippocampus areas that do not participate in the recording procedure. Thus our method does not lose the generality.

In the FSPEEG database three types of activities are considered for investigation: inter-ictal activity signals are selected from the inter-ictal records. Pre-ictal activity signals are chosen from the signals occurring 30 minutes before the seizure onset time up to the seizure onset. Finally, ictal activity signals are selected from the signals between seizure initiation and termination times. As an example, the positions of the electrodes installed in a patient's

¹ <http://epilepsy.uni-freiburg.de>

hippocampus, and two segments of the three-channel ictal and inter-ictal records are displayed in Figure 6.

5.2. Duration of the identification window

In this paper, in order to obtain the coupling matrices corresponding to different activities, ictal and pre-ictal activity signals of three seizures and about three hours of the inter-ictal activity signals of each patient are analyzed. These signals are divided into segments with short duration to be applied in the identification algorithm. This duration must be long enough to cover the dynamics underlying three abovementioned depth-EEG activities. On the other hand, it should not be so long that the assumption of constant parameters along that segment does not hold. Different durations of signals were investigated: one-second, two-second, five-second and ten-second. The identification algorithm is applied to these short segments of signals consecutively.

Actually, for real depth-EEG signals no ground truth is available to determine whether the model parameters are correctly identified or not. Although the value of the cost function (8) (that is proportional to likelihood) can be considered as an important criterion, it cannot indicate the identification performance completely. A more appropriate approach is to reproduce the observed signals via driving the MSMC model by the identified parameters and compare some features of both observed and reproduced signals. In this paper cross spectrum of pairs of signals is taken as a practical criterion that shows how well the model parameters underlying signals are identified (Li et. al., 2011).

For all three activity types, in the sense of Mean Square Error (MSE), the smallest amounts of difference between the cross spectrum of real and reproduced signals are obtained by using “one-second” segment of signals. These average different values are about 0.02 ± 0.005 , 0.04 ± 0.007 , and 0.02 ± 0.01 respectively for inter-ictal, pre-ictal and ictal activities that validate the estimated parameter values. In fact, for the segments longer than one second, the

assumption of constant parameters is not acceptable. On the other hand, according to the frequency content of depth-EEG signals, one-second duration is sufficient to be used in parameter identification algorithms. In Figure 6 an example of one-second signal of each activity is also shown.

5.3. Results of the identification algorithm

The resultant spectral plots of a one-second signal of the ictal activity and those of its corresponding reproduced signal are compared in Figure 7. Similarity of the cross spectra of 3-channel real and reproduced depth-EEG signals is evident from Figure 7. It means that the identified (both extrinsic and intrinsic) parameters are reliable.

Although one-second duration is selected to be the best, some small differences between the spectra are still seen in Figure 7. These errors may be related to the assumed constant value of parameters, neglecting delays in the model and also the unavoidable modeling errors.

As an example of the identification outcome, the estimated signals corresponded to two 10-second segments of inter-ictal and pre-ictal activity signals are displayed in Figures 8a and 8b. The estimated signals are not exactly similar to the real ones, but since the dynamics of real signals are imitated properly, the synthesized signals are acceptable replica of the real world (the average value of difference of real and reproduced signals' cross spectra is about 0.026). For each 1-second segment of signal both identified intrinsic and extrinsic parameters are given in the figure: intrinsic parameters are shown above each channel, and the coupling matrices are shown below the figure.

6. Results: Assessment of different activities' parameters

6.1. Discriminant analysis of extrinsic (coupling) parameters

At first, only the obtained coupling matrices are considered to indicate whether the hippocampal effective synchronization pattern has significant characteristics before seizure occurrence or not.

To this order, according to the coupling matrices obtained for the background activity (interictal signals) of each patient, two onset channels are sorted. This ordering is done such that on average, the channel with the most dominant coupling coefficient toward the other onset channel becomes the first one. Then, the sorted coupling matrices of each activity are averaged over all segments of the same activity. Three average coupling matrices obtained in this manner, are given in equation (12). Components of these matrices are the measure of effective synchronization between depth-EEG channels. For each matrix, the ij th components of the matrices (c_{ij} , $i \neq j$) indicate the influence of the j th channel on the i th channel. The indices $i = 1, 2$ and $j = 1, 2$ correspond to the master and slave in-focus channels, while $i = 3, j = 3$ stand for the out-focus channel:

$$\begin{aligned} M_{\text{inter}} &= \begin{bmatrix} - & 2.42 & 1.93 \\ 1.45 & - & 1.85 \\ 0.67 & 2.14 & - \end{bmatrix} \\ M_{\text{pre}} &= \begin{bmatrix} - & 1.54 & 1.84 \\ 1.35 & - & 1.10 \\ 2.00 & 1.58 & - \end{bmatrix} \\ M_{\text{ictal}} &= \begin{bmatrix} - & 1.13 & 2.92 \\ 2.12 & - & 2.36 \\ 1.96 & 1.45 & - \end{bmatrix} \end{aligned} \tag{12}$$

The variance matrices of each activity type are also obtained. The components of the variance matrices are not trivial, so that the mean coupling matrices, (12), may not be very informative.

Box plot diagrams of Figure 9 show the statistical characteristics of coupling variation during transition to seizure. Each diagram stands for a component of the coupling matrix. The median values of components are shown by small horizontal lines, and the inter-quartile ranges are displayed by the length of each box. Although the median values of each component are different for inter-ictal and pre-ictal activities, these measures cannot suitably discriminate between different activities because of their large variance.

To be more precise, a Quadratic Discriminant Analysis (QDA) classifier is used to indicate the separability of different states. In the discriminant analysis, all six components of the matrix are applied as a feature vector. The performance of the classification procedure is evaluated with a 10-fold cross validation algorithm using 100,000 segments of signals. Distribution of these segments over three classes (inter-ictal, pre-ictal, and ictal) is reported in Table 4. The average percentages of discrimination between pre-ictal/inter-ictal/ictal states are shown in Table 4, in the form of a confusion matrix.

Since the ideal normalized confusion matrix is the identity matrix, the accuracy of recognizing the pre-ictal activity is defined as the mean of diagonal elements of the confusion matrix. This accuracy is about 81.42%, for which specificity in pre-ictal state detection is 98.67%, but the sensitivity is about 56.11%, which is not acceptable.

As well as all six components of the coupling matrix altogether, every component of that matrix are used as the feature, one by one, to determine their importance. Their relevant results are given in Table 4. It is evident from Table 4 that the best effective coupling coefficients are c_{31} and c_{12} , respectively.

This low accuracy of discrimination, as well as the vast variety of coupling coefficients in three states, can be attributed to the fact that seizures can progress with various coupling patterns in different patients. The same result is also obtained for each patient separately (not shown in this manuscript), *i.e.*, even for individual patients the large variances of coupling values and low accuracies of activity separation are observed. This means that the variation of coupling

patterns is not specified to the ictal and pre-ictal activities. For example, during different vigilance states of normal activity the hippocampal coupling values can also change.

6.2. Clustering the Intrinsic Parameters

Through the abovementioned parameter identification procedure, intrinsic parameters of each channel have also been obtained. In this section, we want to evaluate whether these parameters have useful information about an ongoing seizure.

Hence, to indicate the differentiations in the space of the intrinsic parameters of each channel ($\theta_j = [A_j \ B_j \ G_j \ \tau_j]$), a simple clustering scheme is considered here. An attempt is made to cluster the intrinsic parameters of each channel according to the k -means algorithm. For each channel the number of groups, k , is selected as the number for which the squared Euclidian distance between groups is minimum. As a result, intrinsic parameters of two onset channels are clustered into three groups; but for the non-onset channel only one cluster is recognized. These observations correspond to the fact that intrinsic parameters of the non-onset channels do not change significantly and the variation of their activities are only due to the coupling from onset channels.

To see whether the clustering of intrinsic parameters of onset channels can separate different activity types (pre-ictal/inter-ictal/ictal), Table 5 is prepared. Low discriminant power of this clustering approach implies that different activity types are not appeared with significantly different values of intrinsic parameters.

6.3. Discriminant Analysis of both Extrinsic and Intrinsic Parameters

Although it is shown that the hippocampal coupling pattern cannot indicate the pre-ictal activity, we can use the fact of the propagation of pathological state through all areas of

hippocampus, *i.e.*, appearance of seizure state on the non-onset channels without any variation in their intrinsic parameters, to enhance the performance of activity discrimination.

Actually when it is assumed that two different events are responsible to occur before a clinical seizure: *i)* intrinsic parameters of the onset channel take some special values, *ii)* the onset areas' coupling coefficients towards non-onset areas should be increased in such a way that other channels could pursue it, pre-ictal state can be recognized more accurately. This assumption can be interpreted as follow: there are many situations in which the first event occurs, *i.e.*, the onset channels may tend to experience seizure, but because of their insufficient coupling towards other areas, the seizure would be halted, and clinical manifestation of seizure will not be seen. Also, there are many situations in which the hippocampal coupling is high, but there is not a pre-seizure state to be propagated through brain: maybe, not only the pathological activities, but any other activity requires high coupling values to be propagated through brain.

Based on the abovementioned scenario, it seems that taking the intrinsic physiological parameters of the onset channels, besides coupling parameters, into account may provide a considerable amount of useful information.

In this section, by adding the information about the groups to which signals of two onset channels belong, to the “coupling matrix”, the discriminant analysis is repeated. The results are rendered in Figure 10 and Table 6.

In Figure 10 just the role of combining the information about groups of first onset channel to two elements of the coupling matrix (c_{31} and c_{12}) are reported. In this figure, an effort is made to graphically show that the cluster type helps the coupling coefficients to appropriately separate different activities. In Figure 10 the coefficients c_{31} and c_{12} extracted from depth-EEG signals are plotted versus each other. Three clusters of the first onset channel are differentiated by different markers: star (*), circle (o), and cross (x). Also, the activity of pre-ictal, inter-ictal, and ictal segments are respectively specified by red, blue and black colors.

It is evident from Figure 10 that coupling values of three activities are intermingled; on the other hand, some inter-ictal and pre-ictal segments have the same cluster type. However, when both the cluster types and coupling values are considered, the activity classification errors will be negligible: Pre-ictal activity (red color) is almost completely indicated by the ‘o’ cluster type, amounts of c_{3l} larger than 0.045, and amounts of c_{l2} smaller than 3.8. Inter-ictal activity (blue color) is indicated by the ‘x’ cluster type or the ‘o’ cluster type, amounts of c_{3l} smaller than 0.045, and amounts of c_{l2} larger than 3.8. Ictal states are completely characterized by the ‘*’ cluster type. In the same way, other coupling values and cluster number of second onset channel can help to increase the pre-ictal/inter-ictal discrimination accuracy. In Table 6 the results of the 10-fold cross-validation algorithm are summarized. The feature vector contains all components of the coupling matrix and the cluster types of two onset channels, obtained according to their intrinsic parameters. The activity classification performance is reported in the form of a confusion matrix in Table 6. The accuracy, defined as the mean of diagonal elements of the confusion matrix is about 91.33%. The sensitivity of pre-ictal detection versus inter-ictal, that is the main goal of seizure prediction, is 93.51%, and the corresponding specificity is 86.38%.

7. Discussion

According to the demonstrated results in section 6.1, the most specific increment of effective synchronization value was seen in the c_{3l} parameter, for all six patients. This observation can be interpreted as a hypothesis that increment of effective synchronization before seizure is localized to some limited area of brain, which is mainly directional, from an onset area to non-onset ones. This hypothesis is consistent with the seizure prediction methods that try to find the optimized channels for which effective synchronization values have more discriminative

information. However, in this paper it is proposed that finding such informative channels would be much easier, if “effective synchronization values” have been extracted from signals.

Furthermore, according to the results reported in section 6.3, it can be discussed that although variation of the amount of effective synchronization between other channels are not significantly specific, *i.e.* pre-ictal state cannot be characterized by neither increment nor decrement of effective synchronization values, but some events occur uniquely before appearance of a seizure: simultaneous change of onset channel’s intrinsic parameters to maintain seizure-like activity, and increment of that onset channel’s coupling value toward non-onset channels. Taking this suggestion as a property of seizure generation, pre-seizure state has been properly discriminated from inter-ictal state.

8. Conclusion

In this paper, in order to accurately measure the effective synchronization value between different signals of depth-EEG data, a new algorithm based on a computational multi-channel model is introduced. However this algorithm could be applied easily on the real multi-channel depth-EEG signals, for real depth-EEG signals there is no ground truth to decide whether the model parameters are correctly identified or not. Although the value of the cost function (8) (that is proportional to likelihood) can be considered as an important criterion, but it cannot completely indicate the identification performance. Nevertheless, the parameters identified for the observed signals were used in the MSMC model to reproduce them, and then the cross-spectra of pairs of both observed and reproduced signals were compared. The small differences between the cross spectra of 3-channel real and reproduced depth-EEG signals (an average value about 0.026) imply that effective synchronization of different coupled signals have been obtained more accurately than previous methods, which just measure the value of functional (statistical) synchronization (Shayegh et al., 2011).

Although in previous works it is claimed that synchronization of the signals is different for inter-ictal and pre-ictal or ictal states, from the point of this effective synchronization measure and by using FSPEEG database signals, it was found that the coupling matrices cannot suitably discriminate between these activities, because the amount of effective synchronization between depth-EEG channels has high inter- and intra-patient variations during a specific activity. The best accuracy obtained with QDA was about 81.42%, with a slight sensitivity in recognizing the pre-ictal state.

On the other hand, intrinsic parameters of the signals are not significantly different for pre-ictal/inter-ictal activity types. However, by taking both the intrinsic parameters of the onset channels and coupling parameters into account, detection of both pre-ictal and ictal states could be done with higher accuracies (91.33%). In fact, we concluded that coupling between brain areas may be changed in different vigilance and focus states as well as pathological states, but only simultaneous appearance of pathological state on the onset channel, increment of coupling coefficients from onset areas to non-onset ones, and decrement of coupling coefficients toward onset channels is restricted to the time before a seizure occurrence.

9. Acknowledgement

Data for this paper were provided by the Freiburg Seizure Prediction EEG database (FSPEEG). The authors would like to acknowledge the Freiburg Center for Data Analysis and Modeling granting the right of using this database.

The authors would like to acknowledge the Linux lab of Information Technology Center of Isfahan University of Technology (<http://it.iut.ac.ir/>) for executing our MATLAB programs on their clusters.

10. Declaration of interest:

The authors report no conflicts of interest. The authors alone are responsible for the content and writing of the paper.

References

- Ansari-Asl, K., Bellanger, J. J., Bartolomei, F., Wendling, F., & Senhadji, L. (2005). Time-frequency characterization of interdependencies in nonstationary signals: application to epileptic EEG. *Biomedical Engineering, IEEE Transactions on*, *52*(7), 1218-1226.
- Ansari-Asl, K., Senhadji, L., Bellanger, J. J., & Wendling, F. (2006). Quantitative evaluation of linear and nonlinear methods characterizing interdependencies between brain signals. *Physical Review E*, *74*(3), 031916.
- Chávez, M., Le Van Quyen, M., Navarro, V., Baulac, M., & Martinerie, J. (2003). Spatio-temporal dynamics prior to neocortical seizures: amplitude versus phase couplings. *Biomedical Engineering, IEEE Transactions on*, *50*(5), 571-583.
- Da Silva, F. L., Hoeks, A., Smits, H., & Zetterberg, L. H. (1974). Model of brain rhythmic activity. *Kybernetik*, *15*(1), 27-37.
- David, O., Kiebel, S. J., Harrison, L. M., Mattout, J., Kilner, J. M., & Friston, K. J. (2006). Dynamic causal modeling of evoked responses in EEG and MEG. *NeuroImage*, *30*(4), 1255-1272.
- David, O., and Friston, K. J. (2003). A neural mass model for meg/eeg:: coupling and neuronal dynamics. *NeuroImage*, *20*(3), 1743-1755.
- Franaszczuk, P. J., and Bergey, G. K. (1999). An autoregressive method for the measurement of synchronization of interictal and ictal EEG signals. *Biological cybernetics*, *81*(1), 3-9.
- Frei, M. G., Zaveri, H. P., Arthurs, S., Bergey, G. K., Jouny, C. C., Lehnertz, K., Gotman, J., Osorio, I., Netoff, T. I., Freeman, W. J., Jefferys, J., Worrell, G., Le Van Quyen, M., Schiff, S. J., Mormann, F. (2010). Controversies in epilepsy: debates held during the Fourth International Workshop on Seizure Prediction. *Epilepsy & Behavior*, *19*(1), 4-16.
- Friston, K. J., Bastos, A., Litvak, V., Stephan, K. E., Fries, P., & Moran, R. J. (2012). DCM for complex-valued data: Cross-spectra, coherence and phase-delays. *Neuroimage*, *59*(1), 439-455.
- Jouny, C. C., Franaszczuk, P. J., & Bergey, G. K. (2005). Signal complexity and synchrony of epileptic seizures: is there an identifiable preictal period?. *Clinical neurophysiology*, *116*(3), 552-558.
- Le Van Quyen, M., Soss, J., Navarro, V., Robertson, R., Chavez, M., Baulac, M., & Martinerie, J. (2005). Preictal state identification by synchronization changes in long-term intracranial EEG recordings. *Clinical Neurophysiology*, *116*(3), 559-568.
- Li, B., Daunizeau, J., Stephan, K. E., Penny, W., Hu, D., & Friston, K. (2011). Generalised filtering and stochastic DCM for fMRI. *neuroimage*, *58*(2), 442-457.
- Kiebel, S. J., David, O., & Friston, K. J. (2006). Dynamic causal modelling of evoked responses in EEG/MEG with lead field parameterization. *NeuroImage*, *30*(4), 1273-1284.
- Mirowski, P., Madhavan, D., LeCun, Y., & Kuzniecky, R. (2009). Classification of patterns of EEG synchronization for seizure prediction. *Clinical neurophysiology*, *120*(11), 1927-1940.

- Mormann, F., Lehnertz, K., David, P., & Elger, C. (2000). Mean phase coherence as a measure for phase synchronization and its application to the EEG of epilepsy patients. *Physica D: Nonlinear Phenomena*, 144(3), 358-369.
- Mormann, F., Andrzejak, R. G., Kreuz, T., Rieke, C., David, P., Elger, C. E., & Lehnertz, K. (2003). Automated detection of a pre-seizure state based on a decrease in synchronization in intracranial electroencephalogram recordings from epilepsy patients. *Physical Review E*, 67(2), 021912.
- Mormann, F., Andrzejak, R. G., Elger, C. E., & Lehnertz, K. (2007). Seizure prediction: the long and winding road. *Brain*, 130(2), 314-333.
- Netoff, T. I., & Schiff, S. J. (2002). Decreased neuronal synchronization during experimental seizures. *The Journal of neuroscience*, 22(16), 7297-7307.
- Penny, W. D., Litvak, V., Fuentemilla, L., Duzel, E., & Friston, K. (2009). Dynamic causal models for phase coupling. *Journal of neuroscience methods*, 183(1), 19-30.
- Pikovsky, A., Rosenblum, M., & Kurths, J. (Eds.). (2003). *Synchronization: a universal concept in nonlinear sciences* (Vol. 12). Cambridge university press.
- Sakkalis, V., Giurcaneanu, C. D., Xanthopoulos, P., Zervakis, M. E., Tsiaras, V., Yang, Y., Karakonstantaki, E., Micheloyannis, S. (2009). Assessment of linear and nonlinear synchronization measures for analyzing EEG in a mild epileptic paradigm. *Information Technology in Biomedicine, IEEE Transactions on*, 13(4), 433-441.
- Schelter, B., Winterhalder, M., Maiwald, T., Brandt, A., Schad, A., Schulze-Bonhage, A., & Timmer, J. (2006). Testing statistical significance of multivariate time series analysis techniques for epileptic seizure prediction. *Chaos: An Interdisciplinary Journal of Nonlinear Science*, 16(1), 013108-013108.
- Shayegh, F., Amirfattahi, R., Sadri, S., Ansari-Asl, K., & Saraaee, M. H. (2011). Defining a New Measure for Synchronization of Multi-Channel Epileptic Depth-EEG Signals based on Identification of Parameters of a Computational Model. In *Proceedings of the IASTED International Conference July 11-13, Cambridge, United Kingdom* (pp. 344-350).
- Shayegh, F., Bellanger, J. J., Sadri, S., Amirfattahi, R., Ansari-Asl, K., & Senhadji, L. (2013). Analysis of the behavior of a seizure neural mass model using describing functions. *Journal of Medical Signals and Sensors*, 3(1).
- Shayegh, F., Sadri, S., Amirfattahi, R., & Ansari-Asl, K. (2014). A model-based method for computation of correlation dimension, Lyapunov exponents and synchronization from depth-EEG signals. *Computer methods and programs in biomedicine*, 113(1), 323-337.
- Shayegh, F., Sadri, S., Amirfattahi, R., & Ansari-Asl, K. (2013). Proposing a two-level stochastic model for epileptic seizure genesis. *Journal of computational neuroscience*, 1-15.
- Stephan, K. E., Penny, W. D., Moran, R. J., den Ouden, H. E., Daunizeau, J., & Friston, K. J. (2010). Ten simple rules for dynamic causal modeling. *Neuroimage*, 49(4), 3099-3109.
- Wendling, F., Bellanger, J. J., Bartolomei, F., & Chauvel, P. (2000). Relevance of nonlinear lumped-parameter models in the analysis of depth-EEG epileptic signals. *Biological cybernetics*, 83(4), 367-378.
- Wendling, F., Bartolomei, F., Bellanger, J. J., & Chauvel, P. (2002). Epileptic fast activity can be explained by a model of impaired GABAergic dendritic inhibition. *European Journal of Neuroscience*, 15(9), 1499-1508.
- Wendling, F., Ansari-Asl, K., Bartolomei, F., & Senhadji, L. (2009). From EEG signals to brain connectivity: a model-based evaluation of interdependence measures. *Journal of neuroscience methods*, 183(1), 9-18.

Winterhalder, M., Schelter, B., Maiwald, T., Brandt, A., Schad, A., Schulze-Bonhage, A., & Timmer, J. (2006). Spatio-temporal patient–individual assessment of synchronization changes for epileptic seizure prediction. *Clinical neurophysiology*, 117(11), 2399-2413.

<https://epilepsy.uni-freiburg.de/freiburg-seizure-prediction-project/eeg-database>.

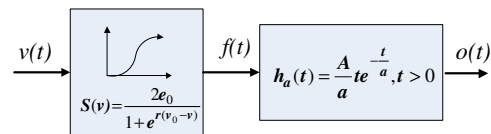


Figure 1. Structure of the neurons as a basis sub-population of the EEG models, the nonlinear static function followed by a linear dynamic transform, respectively at the synapses and soma of the neurons. Accordingly, $f(t) = S(v(t))$ and $o(t) = f(t) * h_a(t)$.

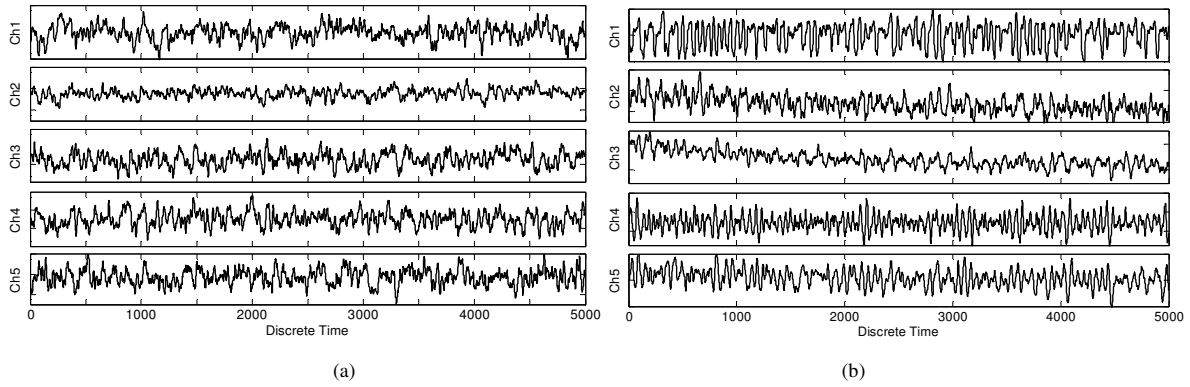


Figure 4. Example of (a) normal and (b) seizure-like signals, respectively synthesized via running the MSMC model by the parameters of the first and second super column of Tables 2 and 3.

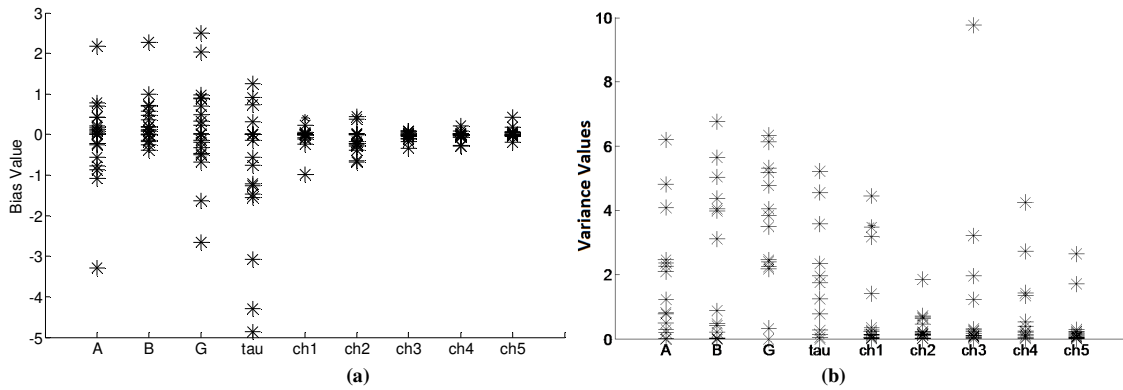


Figure 5. The results of identifying the parameters of five synthetic datasets, I to V, are summarized in this figure, in the form of (a) the bias and (b) the variance of the estimated values. To be more specific, intrinsic parameters of all channels are shown altogether. Also, coupling values of every channel toward other channels are displayed together.

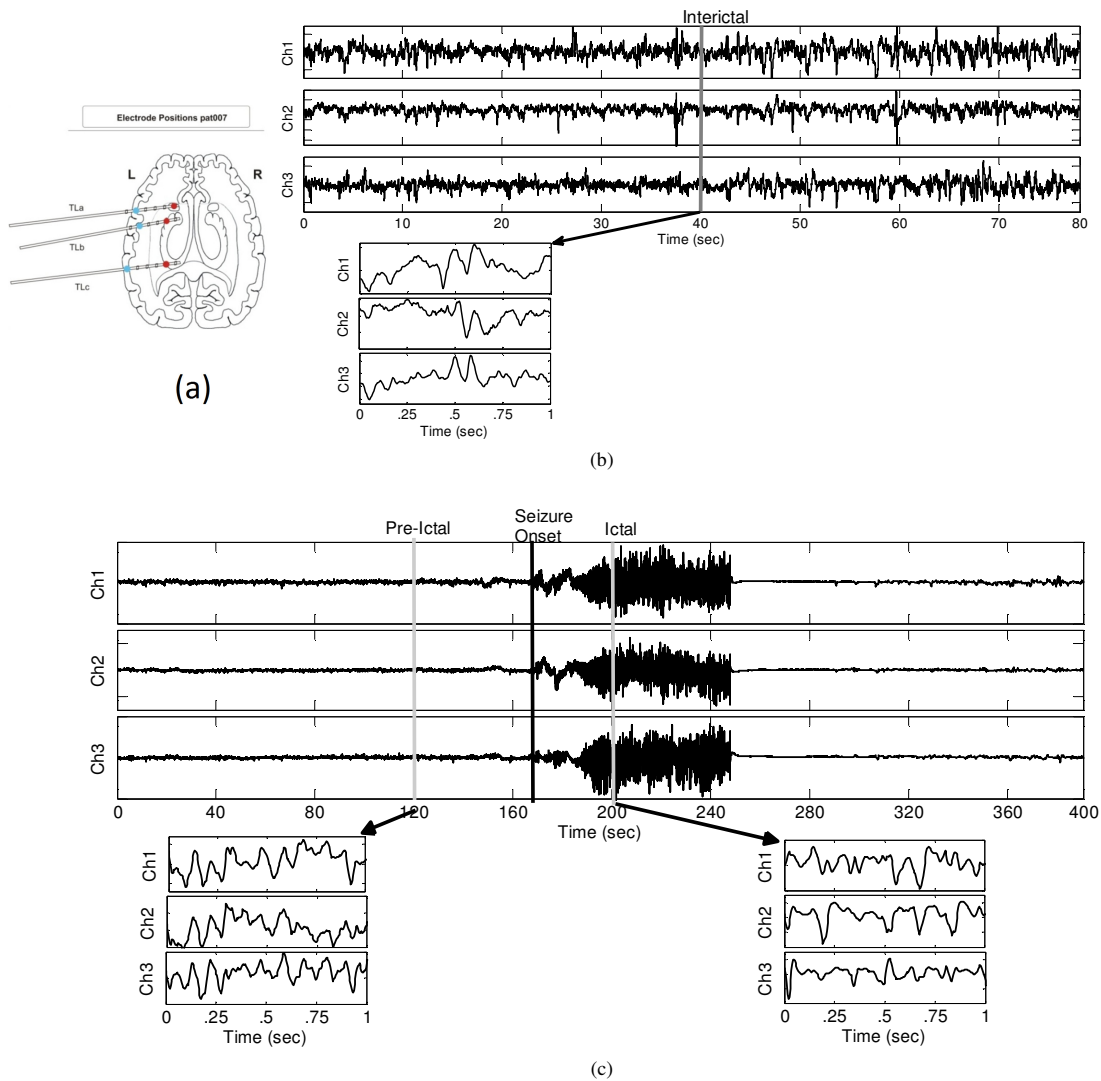


Figure 6. Exemplar multi-channel depth-EEG signals of patient 4 in FSPEEG database. (a) Electrode position (a), (b) about 80 seconds of the inter-ictal record's signals, and (c) about 400 seconds of the ictal record's signals. Three one-second signals of inter-ictal, pre-ictal and ictal activities are zoomed. Such one-second signals are consecutively used to compute the effective synchronization values.

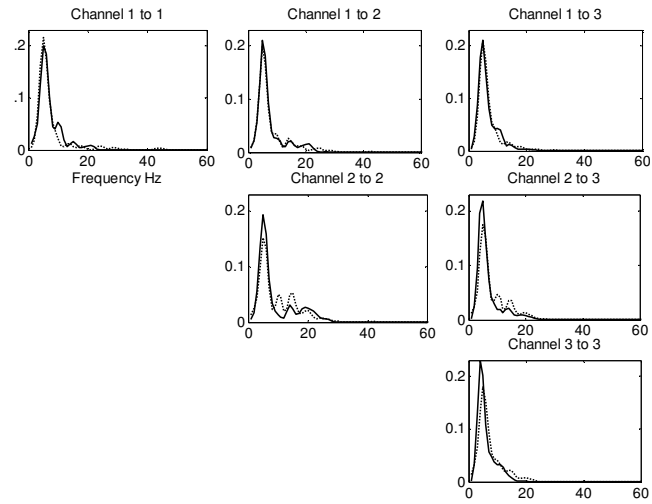
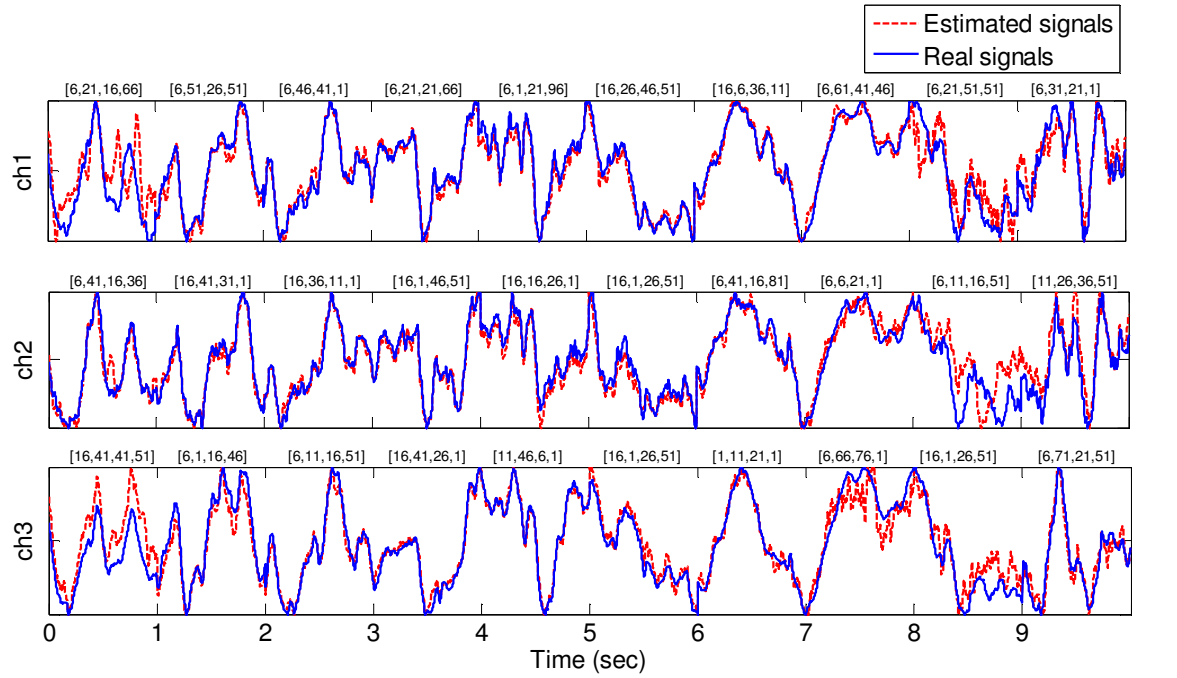
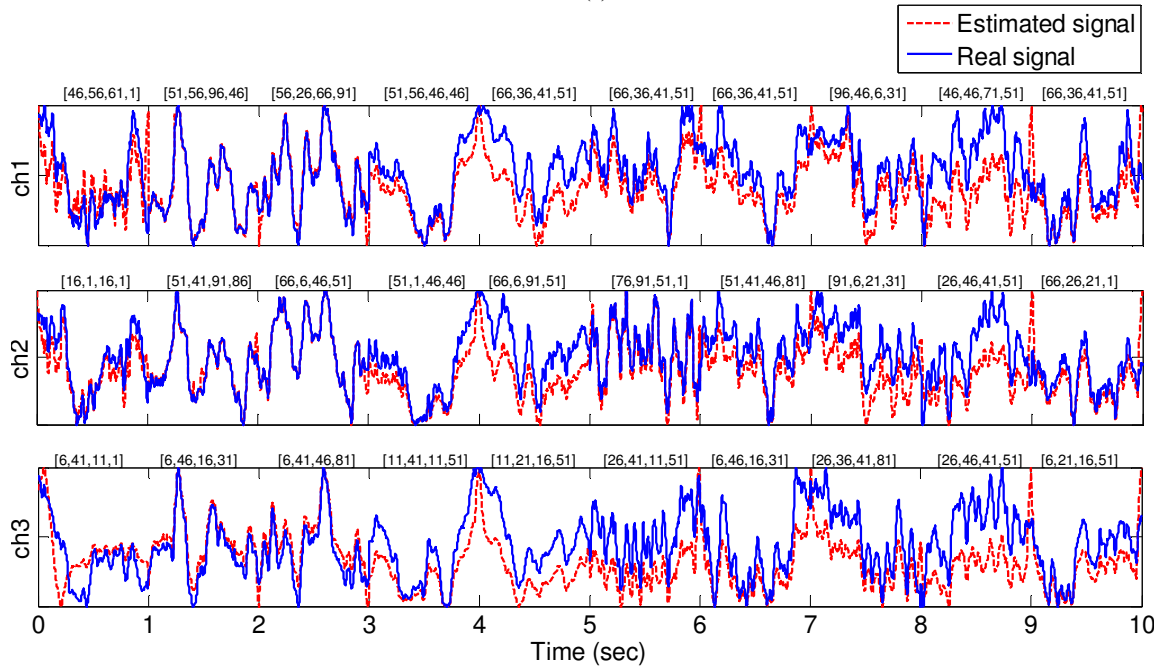


Figure 7. The resultant spectral plots of a one-second real depth-EEG signal of the ictal activity (solid line) and the reproduced signal (dashed line). The cross spectra of 3-channel real and reproduced depth-EEG signals seems to be similar.



$$C: \begin{bmatrix} - & 2.65 & 1.82 & - & 0.14 & 2.09 & - & 3.97 & 1.85 & - & 0.47 & 2.027 & - & 2.86 & 1.95 & - & 0.25 & 2.22 & - & 1.49 & 1.94 & - & 0.63 & 2.04 & - & 2.79 & 1.72 & - & 3.20 & 2.14 \\ 2.03 & - & 2.29 & 1.50 & - & 2.12 & 1.88 & - & 1.94 & 2.36 & - & 2.042 & 0.56 & - & 2.16 & 1.71 & - & 1.82 & 0.88 & - & 1.80 & 1.62 & - & 2.20 & 0.25 & - & 3.11 & 1.40 & - & 2.27 \\ 0.67 & 2.46 & - & 0.50 & 1.69 & - & 0.50 & 2.09 & - & 0.40 & 2.41 & - & 0.57 & 2.68 & - & 0.57 & 3.14 & - & 0.41 & 3.16 & - & 0.58 & 3.58 & - & 0.57 & 2.68 & - & 0.66 & 2.12 & - \end{bmatrix}$$

(a)



$$C: \begin{bmatrix} - & 2.27 & 3.72 & - & 2.66 & 2.25 & - & 2.13 & 3.71 & - & 2.98 & 2.57 & - & 2.61 & 1.36 & - & 3.76 & 1.07 & - & 1.54 & 0.86 & - & 2.88 & 0.60 & - & 1.99 & 0.83 & - & 1.52 & 0.11 \\ 2.08 & - & 2.14 & 1.92 & - & 1.49 & 1.94 & - & 1.39 & 1.69 & - & 1.80 & 1.55 & - & 1.68 & 1.15 & - & 0.60 & 1.94 & - & 1.39 & 1.80 & - & 1.02 & 0.98 & - & 1.92 & 1.18 & - & 2.09 \\ 0.37 & 2.96 & - & 4.22 & 1.50 & - & 4.14 & 3.13 & - & 2.64 & 1.79 & - & 2.54 & 1.89 & - & 3.93 & 2.60 & - & 0.84 & 1.96 & - & 3.48 & 1.64 & - & 1.92 & 1.71 & - & 2.60 & 1.83 & - \end{bmatrix}$$

(b)

Figure 8. Two sample outcomes of the identification procedure: two 10-second signals of inter-ictal and pre-ictal activities of FSPEEG database are plotted by blue line, the identified parameters corresponding to each one-second segment of signals are shown in the figure, and the estimated signals synthesized via driving MSMC model by the identified parameters are plotted by red line. Intrinsic parameters of each channel are shown above them, but the coupling matrices are shown below the figure. (a) inter-ictal signal, (b) pre-ictal signal.

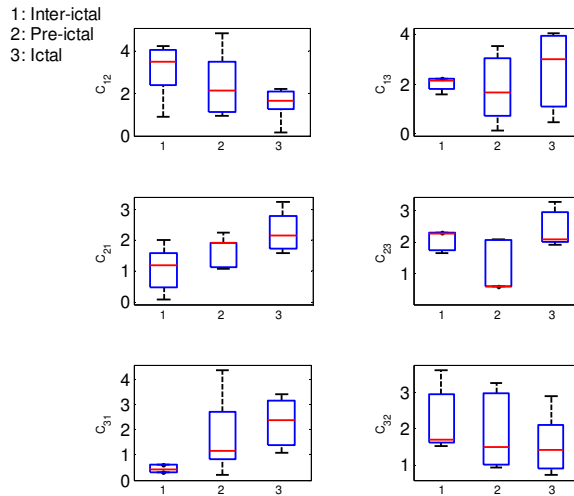


Figure 9. Statistical comparison of coupling coefficients (six components of the coupling matrix) between three different activities (Inter-ictal, Pre-ictal, Ictal). These effective synchronization values are not significant discriminators of different activities

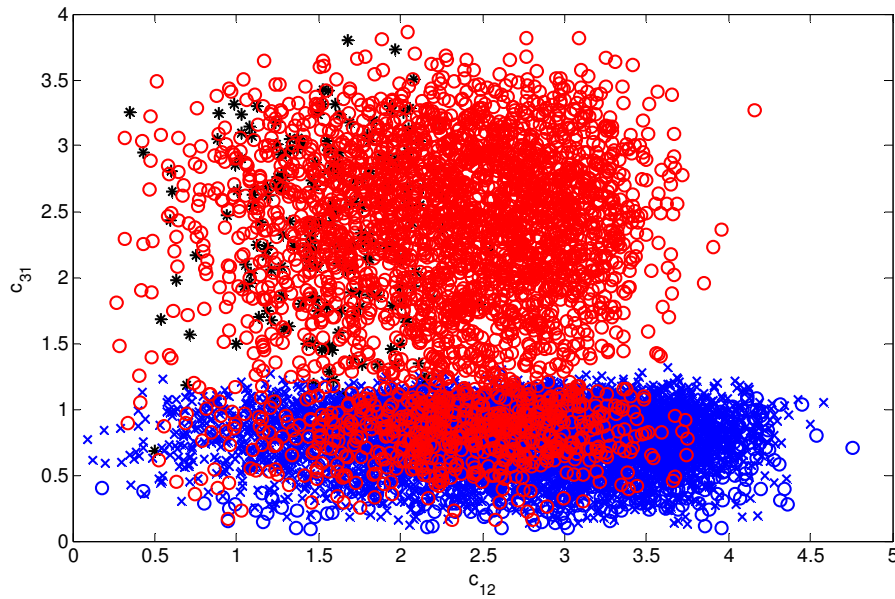


Figure 10. The coupling coefficients c_{31} and c_{12} extracted from depth-EEG signals are plotted versus each other. Three groups obtained by clustering the intrinsic features of the first onset channel are differentiated by different markers: cluster 1 by star (*), cluster 2 by circle (o), and cluster 3 by cross (x). Also, the activity of pre-ictal, inter-ictal, and ictal segments are respectively specified by red, blue and black colors. Since inter-ictal (blue) markers include both ‘o’ and ‘x’, markers cannot indicate the type of activity per se, but one can see that almost all pre-ictal segments, and not other segments, are the circles with c_{31} larger than 0.045 c_{12} smaller than 3.8.

Table 1. Model parameters, interpretation and standard values used to produce background depth-EEG signals (from (Wendling et al., 2002))

Parameter	Interpretation	Standard Value
$1/a$	Dendritic average time constant in the feedback pyramidal excitatory loop	$1/100$ (s)
$1/\tau$	Dendritic average time constant in the feedback excitatory loop of interneurons	$1/100$ (s)
$1/b$	Dendritic average time constant in the slow feedback inhibitory loop	$1/50$ (s)
$1/g$	Somatic average time constant in the fast feedback inhibitory loop	$1/500$ (s)
C_1, C_2	Average number of synaptic contacts in the excitatory feedback loop	$C_1=135, C_2 = 108$
C_3, C_4	Average number of synaptic contacts in the slow feedback inhibitory loop	$C_1=C_3 = 33.75$
C_5, C_6	Average number of synaptic contacts in the fast feedback inhibitory loop	$C_1=40.5, C_2 = 13.5$
C_7	Average number of synaptic contacts between slow and fast inhibitory interneurons	$C_7=108$
e_0, v_0, r	Parameters of the nonlinear asymmetric sigmoid function	$v_0=6$ (mV) $e_0=2.5$ (s ⁻¹) $r=.56$ (1/mV)

Table 2. The correct (Left columns) and identified (Right column) intrinsic parameter values of the five areas of synthetic data sets I (first super-row) and II (second super-row). Each dataset contains signals generated via 200 different runs of the MSMC model by these intrinsic values and extrinsic values of Table 3. One example signal of each data set is shown in Fig 4.

		True intrinsic parameters				Identified intrinsic parameters			
		<i>A</i>	<i>B</i>	<i>G</i>	τ	<i>A Mean Variance</i>	<i>B Mean Variance</i>	<i>G Mean Variance</i>	τ Mean Variance
Dataset I	Ch1	9	1	61	100	9.0000 0.0000	1.0000 0.0000	61.0000 0.0000	100.00 0.0000
	Ch2	3.25	22	10	100	4.0387 0.4957	22.7077 6.7625	10.9011 4.0470	98.4511 0.0478
	Ch3	3	22	10	100	3.2154 0.7716	21.9857 4.3681	10.2327 3.8414	95.7092 1.9635
	Ch4	10	5	65	100	10.0856 4.8138	5.3635 0.2147	65.8872 6.3341	98.7812 3.5723
	Ch5	3	20	8	100	5.1886 2.4645	20.1265 3.9778	10.0400 5.3164	99.4345 0.2712
Dataset II	Ch1	3.25	22	10	100	3.2869 0.0005	22.0000 0.0000	12.5116 2.2426	98.5226 0.7760
	Ch2	3.25	22	10	100	3.4234 0.3013	24.2793 5.0493	9.5045 2.4598	96.9279 4.5547
	Ch3	3	30	38	100	2.7849 0.8218	29.8670 0.4854	37.6881 5.1920	100.0000 0.0000
	Ch4	15	25	25	65	15.4274 0.1187	25.7223 4.2597	25.4973 3.5328	63.7334 2.4271
	Ch5	50	50	65	30	50.4327 0.1356	50.1996 2.5263	65.7100 0.1200	30.3139 2.1252

Table 3. The correct (Left columns) and identified (Right column) extrinsic (coupling coefficients between five areas) of synthetic data sets I (first super-row) and II (second super-row). Each dataset contains signals generated via 200 different runs of the MSMC model by these extrinsic values and intrinsic values of Table 2. One example signal of each data set is shown in Fig 4.

		True coupling values					Identified coupling values				
		Ch1	Ch2	Ch3	Ch4	Ch5	Ch1 Mean Variance	Ch2 Mean Variance	Ch3 Mean Variance	Ch4 Mean Variance	Ch5 Mean Variance
Dataset I	Ch1		2	3	4	5		1.8667 0.0159	2.9989 0.0166	3.9943 0.0161	4.9821 0.0178
	Ch2	25		6	5	7	25.4059 3.5458		5.6727 1.9613	4.7121 4.2406	7.0590 1.7223
	Ch3	5	5		11	2	4.0145 4.4620	4.7088 1.8641		10.7250 2.7278	1.8114 2.6550
	Ch4	1	4	5		17	0.9218 0.0327	3.7781 0.0206	4.9859 0.0141		17.0060 0.0147
	Ch5	9	0	7	8		8.7664 1.4066	-0.1682 0.6321	7.0798 1.2319	8.2144 1.4347	
Dataset II	Ch1		3	4	6	1		3.0068 0.0226	3.9776 0.1004	5.9755 0.2052	0.9721 0.0226
	Ch2	7.5		36	15	6	7.3914 3.4720		35.8354 9.7723	14.9374 1.3432	6.1787 0.1397
	Ch3	10	2.4		8.8	38	10.2411 0.1607	2.4274 0.1398		8.8822 0.5335	38.4249 0.1675
	Ch4	1.5	5.5	3.5		2.5	1.5045 3.1773	5.4878 0.1675	3.5015 3.2224		2.5565 0.2396
	Ch5	3	10	4.33	2.66		3.0580 0.2638	10.0209 0.2397	4.2849 0.2664	2.6588 0.2615	

Table 4. The results of the quadratic discriminant analysis obtained in a 10-fold cross validation manner. In the first analysis, different components of the coupling matrix are used altogether as a feature vector. Then each of them is considered as a feature, individually.

	Features	All six components of coupling matrix			c_{12}		
	Number of segments	Inter-ictal	Pre-ictal	Ictal	Inter-ictal	Pre-ictal	Ictal
Inter-ictal	65,600	88.67%	0.53%	0.79%	45.73%	36.14%	18.12%
Pre-ictal	32,400	18.92%	56.11%	24.97%	19.97%	50.00%	30.03%
Ictal	2,000	3.50%	7.00%	89.50%	0%	6.00%	94.00%

	Features	c_{13}			c_{21}		
	Number of segments	Inter-ictal	Pre-ictal	Ictal	Inter-ictal	Pre-ictal	Ictal
Inter-ictal	65,600	43.13%	44.60%	12.27%	55.60%	34.42%	9.98%
Pre-ictal	32,400	31.97%	63.07%	4.96%	33.52%	52.47%	14.01%
Ictal	2,000	10.90%	12.50%	76.60%	8.60%	12.55%	21.15%

	Features	c_{23}			c_{31}		
	Number of segments	Inter-ictal	Pre-ictal	Ictal	Inter-ictal	Pre-ictal	Ictal
Inter-ictal	65,600	52.89%	37.02%	10.09%	89.40%	0.59%	0.01%
Pre-ictal	32,400	28.16%	49.21%	22.63%	19.38%	57.69%	22.93%
Ictal	2,000	6.85%	7.65%	85.50%	4.05%	61.95%	34.00%

	Features	c_{32}		
	Number of segments	Inter-ictal	Pre-ictal	Ictal
Inter-ictal	65,600	49.69%	38.42%	11.89%
Pre-ictal	32,400	20.71%	65.34%	13.95%
Ictal	2,000	19.55%	31.10%	49.35%

riminators of different activities

Table 5. The results of clustering the intrinsic parameters of onset channels.

		Inter-ictal	Pre-ictal	Ictal
Inter-ictal	65,600	61.72%	27.65%	10.63%
Pre-ictal	32,400	16.55%	73.13%	10.32%
Ictal	2,000	1.34%	1.32%	97.24%

Table 6. The results of the quadratic discriminant analysis obtained in a 10-fold cross validation manner. The feature vector contains both extrinsic and intrinsic parameters.

	Features	All extrinsic and intrinsic parameters		
	Number of segments	Inter-ictal	Pre-ictal	Ictal
Inter-ictal	65,600	85.23%	13.44%	1.33%
Pre-ictal	32,400	6.36%	91.72%	1.92%
Ictal	2,000	1.23%	1.71%	97.06%

